

CAAP Annual Report

Date of Report: 04/30/2024

Prepared for: U.S. DOT Pipeline and Hazardous Materials Safety Administration

Annual Period: From (April 1, 2023) to (March 31, 2024)

Contract Number: 693JK32250001CAAP

Project Title: *Selection and Development of Safer Polymer and Composite Pipeline Liners through Microstructural and Macroscopic Study of Materials and Designs*

Prepared by: *Dr. Vikas Srivastava (PI*), Dr. Ryan Poling-Skutvik, Dr. Edith Mathiowitz*

Contact Info.: **Email: vikas_srivastava@brown.edu
Phone: 401-863-2863*

Table of Contents

1.	Background and Objectives in the 1 st Annual Report Period	5
1.1.	Background.....	5
1.2.	Objectives in the 1 st Annual Report Period.....	5
1.2.1.	Literature Review of Existing Polymers and Characterization.....	5
1.3.	We aimed to study the literature and synthesize information for pipeline liner polymers of interest. A summary of key papers is presented in Table 3.....	5
	Table 3. Selected useful literature.....	6
1.3.1.	Polymer Selection for Experimental Studies	7
1.4.	Table 4. Polymers for experimental studies.....	7
1.4.1.	Microstructure Characterization	7
1.4.2.	Characterization of Thermal Properties	7
1.4.3.	Mechanical Characterization of unaged liner polymers	7
2.	Experimental Program in the 1 st Annual Report Period	8
2.1.	Experimental Design.....	8
3.	Results and Discussions.....	11
4.	Future work.....	23

Section A: Business and Activities

(a) Contract Activities

- Contract Modifications:

None

- Educational Activities:

- Student mentoring:

PhD Student Mohammadjavad Hajirezaei has been trained on DSC, DMA and rheology. Moreover, to prepare standard samples, a hydraulic press is utilized to manufacture standard samples in accordance with ASTM standards. The optimization of these processing conditions has been conducted by him,, and undergraduate researchers Maile Campbell and Aiden Ferreira.

PhD Student Zakhar Lyakhovych has been trained on DSC, XRD, PLM and FTIR. He has established protocols for testing of both meltcast and preprocessed samples. Undergraduate students at the lab have been taught how to use XRD and FTIR and have begun to learn how to extract morphological information from the data.

PhD student Deepto Ghosh has been officially onboarded on the project. He has been trained on the MTS servo-hydraulic mechanical testing machine. Another graduate student, Kevin LoGiudice, is helping Deepto with the experimental design of the creep test set-up and mechanical test plans.

All students have been onboarded to this research project and have been learning about pipeline materials, safety and integrity challenges, including rehabilitation considerations. You can find more detailed work by these students in the technical section of this report.

(b) Financial Summary

- Federal Cost Activities:

The PI, co-PIs and student project year 1 involvement, materials and supplies, cost-share facility expense and travel for Brown University and University of Rhode Island are summarized in Table 1.

- Cost share contribution:

Table 2 below details the cost share by Brown University and the University of Rhode Island for year 1 of the research project.

Table 1. Summary of Yr 1 Spending				
Institution		Amount (\$)	Amount (\$)	Subtotal (\$)
Brown University	Category	Salary (\$)	Fringe (\$)	
	Salaries	50,539.20	7,141.00	57,680.20
	Graduate Student Fees			8,769.95
	Facility Usage			4,013.75
	Purchased Services			4,320.06
	Materials and Supplies			2,225.08
	Travel			1,068.46
	Total Direct			78,077.50
	Indirect			56,112.97
	Subtotal			134,190.47
University of Rhode Island	Personnel	Salary (\$)	Fringe (\$)	
	Salaries	7,700.08	381.45	8,081.53
	Operating Expenditures			9,292.45
	Travel			4,089.26
	Student Aid			2,438.30
	Total Direct			23,901.54
	Indirect			12,341.38
	Subtotal			36,242.92
Total			170,433.39	

Table 2. Summary of Yr 1 Cost Share				
Institution		Amount (\$)	Amount (\$)	Subtotal (\$)
Brown University	Category	Salary (\$)	Fringe (\$)	
	Graduate Student Tuition			24,796.11
	Subtotal			24,796.11
University of Rhode Island	Direct Costs			11,283.15
	Indirect			4,273.77
	Subtotal			15,556.92
Total				40,353.03

(c) Project Schedule Update

- Project Schedule:

The project has started for year 1 as planned and focused on developing the experimental methods, establishing experimental set-ups and early characterization of the polymers.

- Corrective Actions: N/A

Section B: Detailed Technical Results in the Report Period

1. Background and Objectives in the 1st Annual Report Period

1.1. Background

Cast iron pipes carrying natural gas have been in service for several decades in the United States. A significant portion of these vintage cast iron pipes are primarily located in disadvantaged areas of older cities and towns and are prone to damage, corrosion, cracks, and leaks. Carbon dioxide and hydrogen sulfide in the natural gas, in combination with moisture, can result in sweet and sour corrosions. This has a deleterious effect on the host iron pipe leading to mechanical strength and property degradation. Open excavation and replacement of these deteriorating pipes are prohibitive due to the lack of access as well as the high cost associated with excavation and restoration. As an alternative, the rehabilitation of these pipelines can be achieved by trenchless technology [1,2] using an internal structural liner. The structural liner must possess high corrosion resistance, high strength-to-weight ratio, long-term mechanical durability in hydrocarbon and pressure environments, and flexibility to operate in trenchless insertion into the host pipe. The use of internal structure liners is an easy fix for rehabilitating cast iron pipes carrying natural gas for decades as opposed to open excavation and replacement of these deteriorating pipes. Commonly used polymers for these liners are high-density polyethylene (HDPE), polyamides (PA), polyvinylidene difluoride (PVDF) and cured-in-place glass fiber *epoxy* composites [3–6]. However, a comprehensive study pertaining to the changes in the morphology and microstructure of these polymers under chemical exposure (hydrocarbons with the presence of moisture) and how it accelerates the degradation of the mechanical and structural properties of the liner material is lacking. Hence, such a study will enable us to make informed predictions about the expected operational lifetime of the liner material.

1.2. Objectives in the 1st Annual Report Period

1.2.1. Literature Review of Existing Polymers and Characterization

1.3. We aimed to study the literature and synthesize information for pipeline liner polymers of interest. A summary of key papers is presented in Table 3.

Table 3. Selected useful literature

Title	Year	Polymer	Testing	Notes	Link
Effect of Crystallinity of Polyethylene with Different Densities on Breakdown Strength and Conductance Property ¹	2019	Polyethylene	DSC, XRD	Comparison of LLDPE, LDPE, MDPE, HDPE	Link
Crystallinity of Linear Low Density Polyethylene and of Blends with High Density Polyethylene ²	1986	Polyethylene	Microscopy, DSC	Made crystalline observations through regular microscopy	Link
Mesophases in polyethylene, polypropylene, and poly(1-butene) ³	2010	Polyethylene, Polypropylene, Poly(1-butene)	DSC, XRD, PLM	Summarizes several investigations into crystallinity and intermediate phases	Androsch, et al.
Comparative Characterization of Hot-Pressed Polyamide 11 and 12: Mechanical, Thermal and Durability Properties ⁴	2021	PA11, PA12	FTIR, DSC, XRD	Links microstructure characteristics to mechanical tests	Link
Study on crystal structure and phase transitions of polyamide 12 via wide-angle X-ray diffraction with variable temperature ⁵	2020	PA12	XRD	Created and analyzed several crystal forms of PA12	Link
Glass transition temperature versus structure of polyamide 6: A flash-DSC study ⁶	2012	PA6	DSC, XRD		Link
Rheo-optical FTIR Spectroscopy of Epoxy Resins ⁷	1995	Epoxy	FTIR	Included thermal and mechanical analysis	Link
Creep of epoxy–clay nanocomposite adhesive at the FRP interface: A multi-scale investigation ⁸	2014	Epoxy	FTIR, XRD, DSC	Mechanical analysis included sheer and creep tests	Link
Effect of heat-treatment temperature after polymer melt and blending ratio on the crystalline structure of PVDF in a PVDF/PMMA blend ⁹	2013	PVDF	FTIR, XRD, DSC		Link

1.3.1. Polymer Selection for Experimental Studies

1.4. Table 4. Polymers for experimental studies

Polymer	Product Name	Type	Source
PVDF	Fluorinar-C PVDF	Filament	Nile Polymers
	PVDF	Sheet	McMaster-Carr
Epoxy Resin	Thin Epoxy Resin	Liquid	Composite Envisions
	3:1 Epoxy Hardener - Medium Cure	Liquid	Composite Envisions
Glass Fibers	1/4 Inch Chopped Fiber Glass Strands	Short fibers	Simond Store
Polyethylene	Polyethylene - High Density	Granules	Sigma-Aldrich
	HDPE	Sheet	US Plastics
Polyamide	Nylon (PA12) Powder	Powder	Sintratec
	Polyamide	Sheet	McMaster-Carr

1.4.1. Microstructure Characterization

- 1.4.1.1. Establish a procedure for performing X-ray diffraction testing and ATR-FTIR to establish phase contents and indications of crystal structure. Obtain information related to control and unprocessed samples to use as t=0 metrics for comparison to aged and mechanically tested samples

1.4.2. Characterization of Thermal Properties

- 1.4.2.1. Establish the feasibility of DSC as a method that would be able to analyze the range of samples that we are testing. Establish testing procedures as well as preliminary thermal profiles of samples before they are processed.

1.4.3. Mechanical Characterization of unaged liner polymers

- 1.4.3.1. Extract the mechanical properties of the chosen polymer samples through tension testing. Establishing a model for the creep test setup.

2. Experimental Program in the 1st Annual Report Period

2.1. Experimental Design

2.1.1. Sample preparation

The production of standard sample geometries, including dog-bone, rectangular and disk (Table 5) from the various polymers of interest for the experiments is required. Powders and pellets can be processed and converted into polymer test samples using a thermal hydraulic press. Hydraulic press (Figure 1) requires precise procedures due to the necessity of controlling temperature, pressure, and time. While these are the primary factors, additional considerations include preheating, cooling rate, and duration.

Table 5. Various sample geometries

Samples	Standard
Dog-bone	ASTM D638-22- Type v
Rectangular	ASTM D790-17
Disk	Based on rheometer parallel plate disks (8, 20 and 25 in diameters)



Figure 1: The left picture shows the hydraulic press machine, and the right one shows the molds and manufactured samples.

2.1.2. Thermal analysis

Differential Scanning Calorimetry (DSC) is a technique for measuring the thermal properties of polymeric and other materials. This analysis is conducted using a TA Instrument, typically involving a small quantity of the sample. DSC determines the temperature and heat flow associated with material phase transitions as a function of both time and temperature. During alterations in temperature, DSC quantifies the heat exchanged by the sample, either absorbed or emitted, relative to a reference material, establishing a temperature gradient between the sample and the reference. The primary parameters commonly derived from DSC measurements include the melting temperature (T_m), glass transition temperature (T_g), crystallization temperature (T_c), and crystallinity which is calculated through:

$$\% \text{ crystallinity} = \frac{\Delta H_M}{\Delta H_{100\%}} \times 100$$

2.1.2. Time-Temperature superposition (TTS) principle

The mechanical characteristics of viscoelastic materials are influenced by temperature. The data obtained at varying temperatures can be shifted relative to a reference frequency, aligning curves from different temperature conditions to create a unified master curve. This master curve serves as a reference for extracting specific material properties under any given condition [23] and also quantifies the activation energy of dynamic processes. This time-temperature superposition concept is presented in Figure 2.

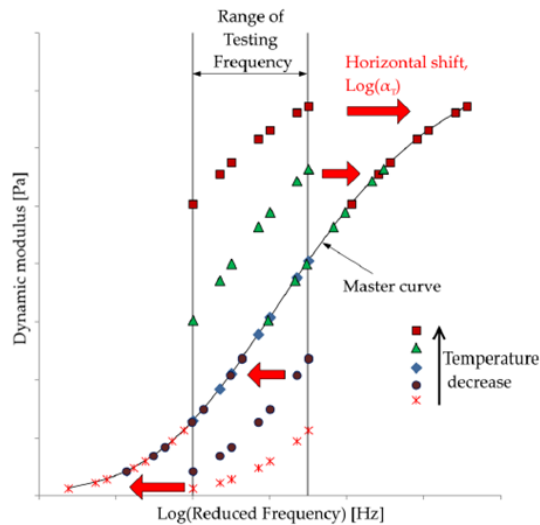


Figure 2: The concept of the time-temperature superposition (TTS) principle and master curve formation [22].

The temperature dependence of the shift factor can be studied using the Arrhenius and the WLF (Williams, Landel and Ferry) equations. The WLF equation is generally applicable in the temperature range up to $T_g + 100$ °C. For higher temperatures, the shift factor closely follows an Arrhenius-type equation [24]:

$$\ln(a_T) = \frac{E_a}{R} \left(\frac{1}{T} - \frac{1}{T_{ref}} \right)$$

where a_T is the shift factor, R is the universal gas constant, E_a is the activation energy of flow, T is the experimental temperature, and T_{ref} is the reference temperature.

2.1.3 Tensile Testing

Dogbone-shaped samples were cut from polymer sheets. These samples were then used for tension testing in an MTS machine (Figure 3) to determine the elastic modulus and yield strength. Then, tension tests were conducted on these samples at a slow strain rate of 0.0005 s^{-1} . Additional tests were performed to show rate (inverse of time) dependent behavior of these polymers.

Table 6. Sample Geometries used for tensile testing

Material	Standard
HDPE	ASTM D638-14- Type V
PA	ASTM D638-14- Type I
PVDF	ASTM D638-14- Type I

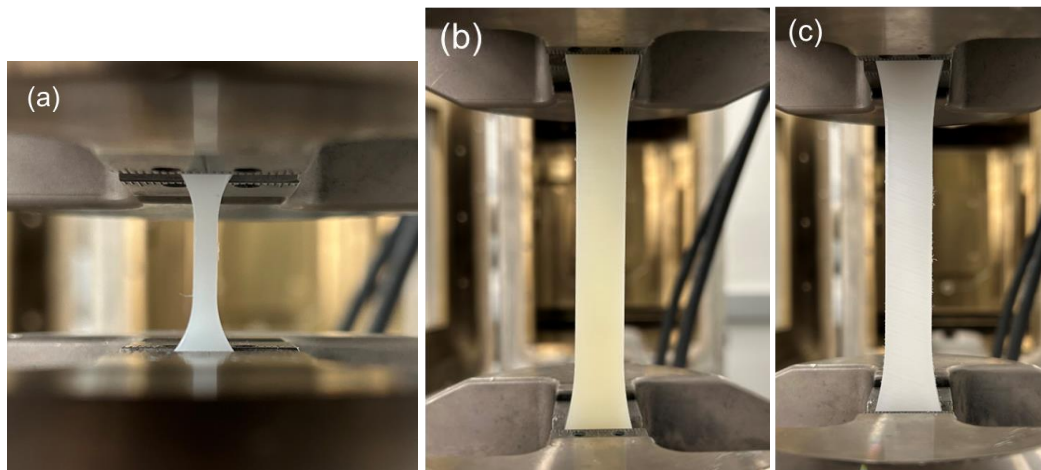


Figure 3: Samples Loaded on an MTS Machine (a) HDPE, (b) PA, and (c) PVDF.

3. Results and Discussions

3.1. Hot pressing

The process, known as hot pressing, presented inherent challenges due to potential defects that could arise in the samples. We identified key variables to mitigate these effects, including temperature, duration, and pressure applied by the hydraulic press. Optimization of these variables is crucial to produce appropriate samples for the next experiments. Figure 4 illustrates several sample preparations conducted under various experimental variables. High-quality samples were identified through the analysis of rheological data, as well as through physical observation and comparison with other samples. It is noteworthy that with increasing temperature and pressure, the quality of the samples tends to improve. Elevated temperatures allow for the plastic to more fully settle into the mold shape, while aiding in the easier displacement of air bubbles and cavities to the surface. Additionally, higher pressures ensure the sample is pressed into the mold completely and that all air is evacuated from the mold and plastic.

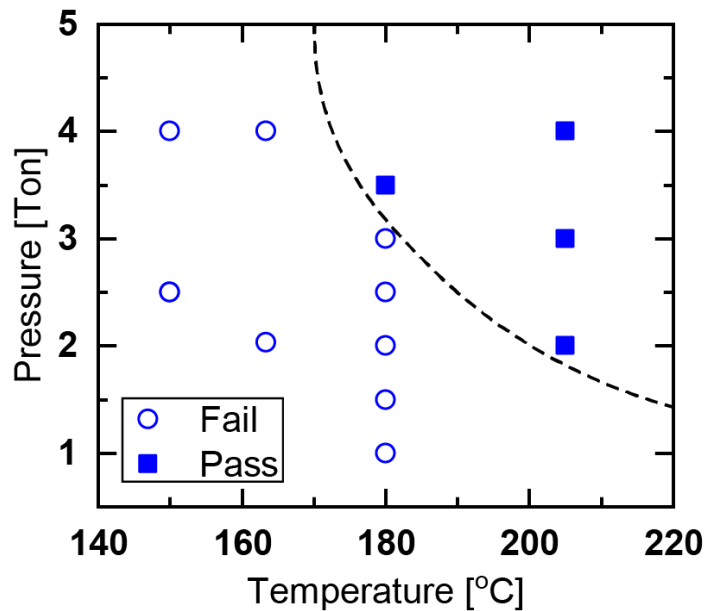


Figure 4: Sample preparation under various pressures and temperatures.

3.2. Differential Scanning Calorimetry

DSC graphs of the materials are shown in Figure 5. It is obvious that PA has the highest melting temperature. The melting temperature obtained from these graphs is used to determine the optimal temperature for sample preparation, particularly considering our utilization of a hot press

procedure conducted at temperatures significantly surpassing the melting temperature, as explained in Figure 4. The temperatures and melting enthalpies also help provide more specifics about the type of polymer being analyzed. In the case of the high melting point of the polyamide, it indicates that it is a shorter polyamide chain likely PA6 or PA66. Epoxy, being a thermoset polymer, displays no thermal events on a DSC scan.

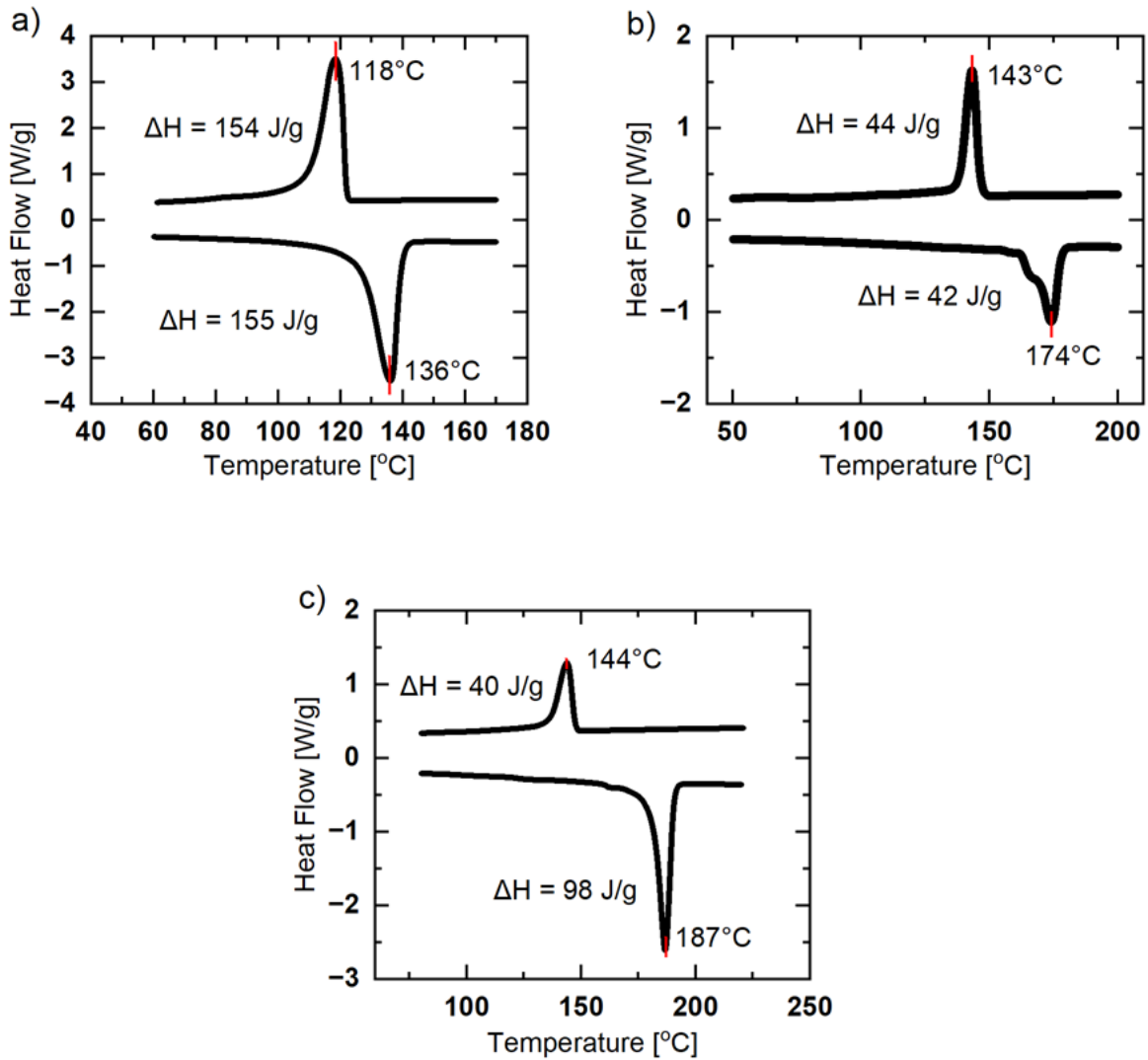


Figure 5: DSC graphs of (a) HDPE, (b) PVDF and (c) PA.

Table 7. Experimental thermal properties of thermoplastic and crystalline content

Material	Melt Temperature (J/g)	Experimental Enthalpy (J/g)	100% crystalline Enthalpy (J/g)	% Crystallinity
HDPE	136	155	292 ¹⁹	53.1%
PVDF	174	42	105 ²⁰	40.0%
PA	187	98	226 ²¹	43.4%

3.3. Time-Temperature superposition

TTS was performed on HDPE and PVDF samples. The results are shown in Figure 6.

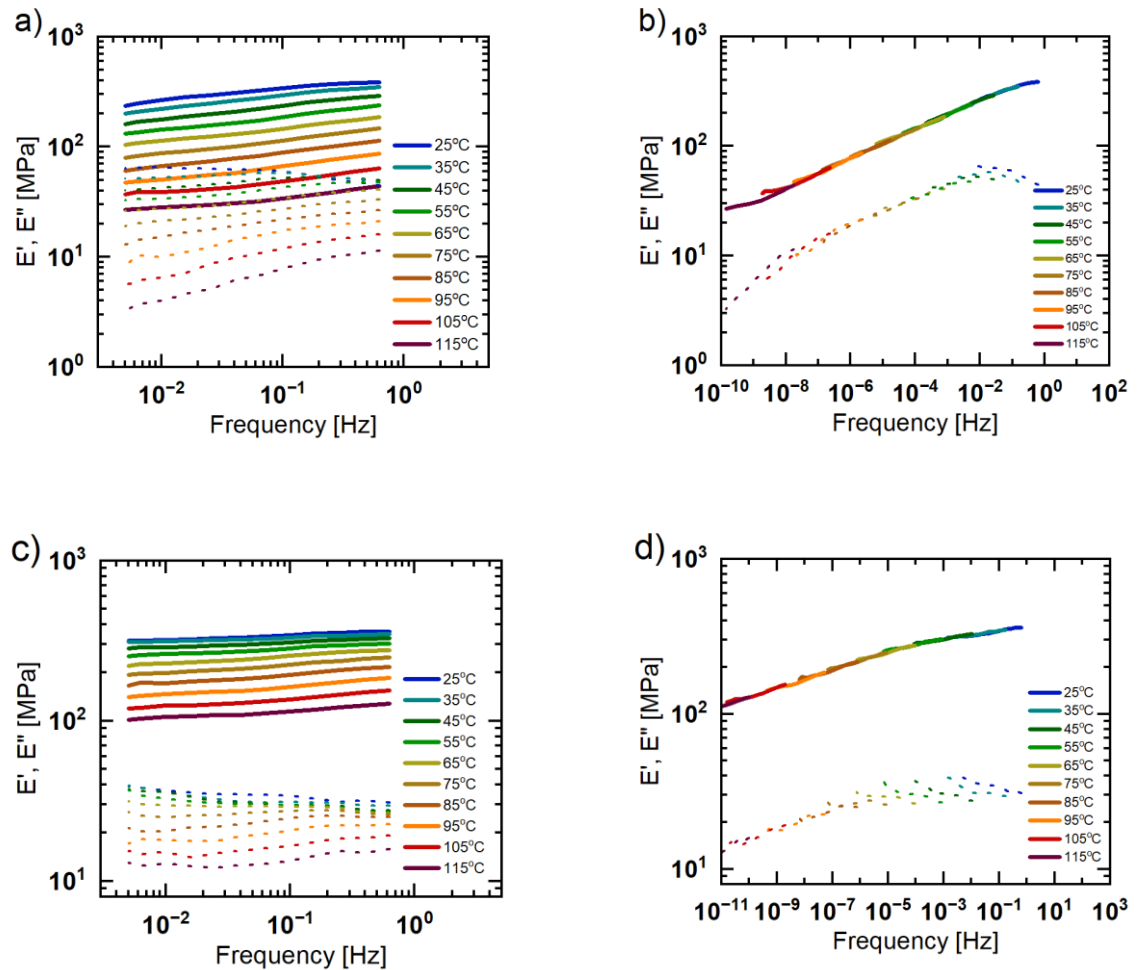


Figure 6: (a) Storage and loss modulus of HDPE at various temperatures (a) HDPE and (c) PVDF. Master curves (b) HDPE and (d) PVDF.

The assumption that all relaxation times are affected by temperature to the same extent does not always hold. Processes like crosslinking, degradation, and depolymerization are not necessarily affected in the same way over the whole temperature range under investigation. The same is true for multi-phase polymers. The shift factors of HDPE and PVDF are shown in Figure 7 based on their master curves.

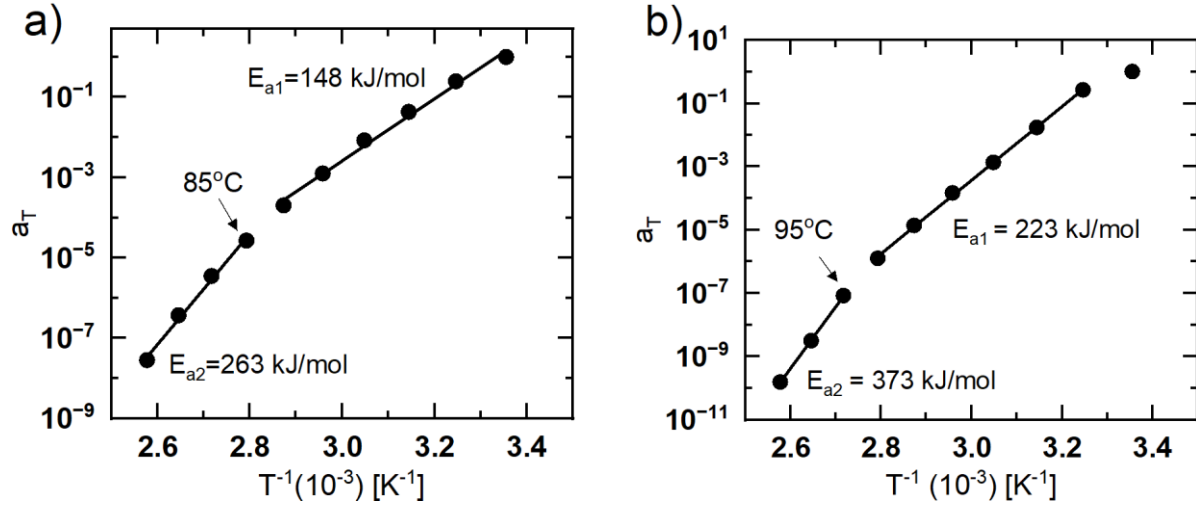


Figure 7: (a) HDPE shift factor and (b) PVDF shift factor.

It is our belief that activation energy is a variable that can significantly be influenced by the aging of polymers under varying gas compositions and pressures. We expect that infiltration of the polymer by gas will increase dynamic relaxations and reduce activation energies. Thus, by tracking changes in the activation energy over different exposure protocols, we can assess degradation of polymer properties more robustly and precisely.

The operation lifetime of these polymers can be forecasted by utilizing the shift factors presented in Figure 6 particularly at elevated temperatures. Certain datasets extracted from HDPE graphs and equation below are presented in Table 8.

$$\tau_{T_{ref}} = \frac{\tau_T}{a_T}$$

Table 8. HDPE predicted operating times based on its shift factors

1 day aging time at various temperatures [°C]	Predicted operating time at 25°C
35	4 days
45	24 days
55	121 days
65	806 days
75	14 years
85	102 years

3.4 Attenuated Total Reflectance-Fourier Transform Infrared (ATR-FTIR)

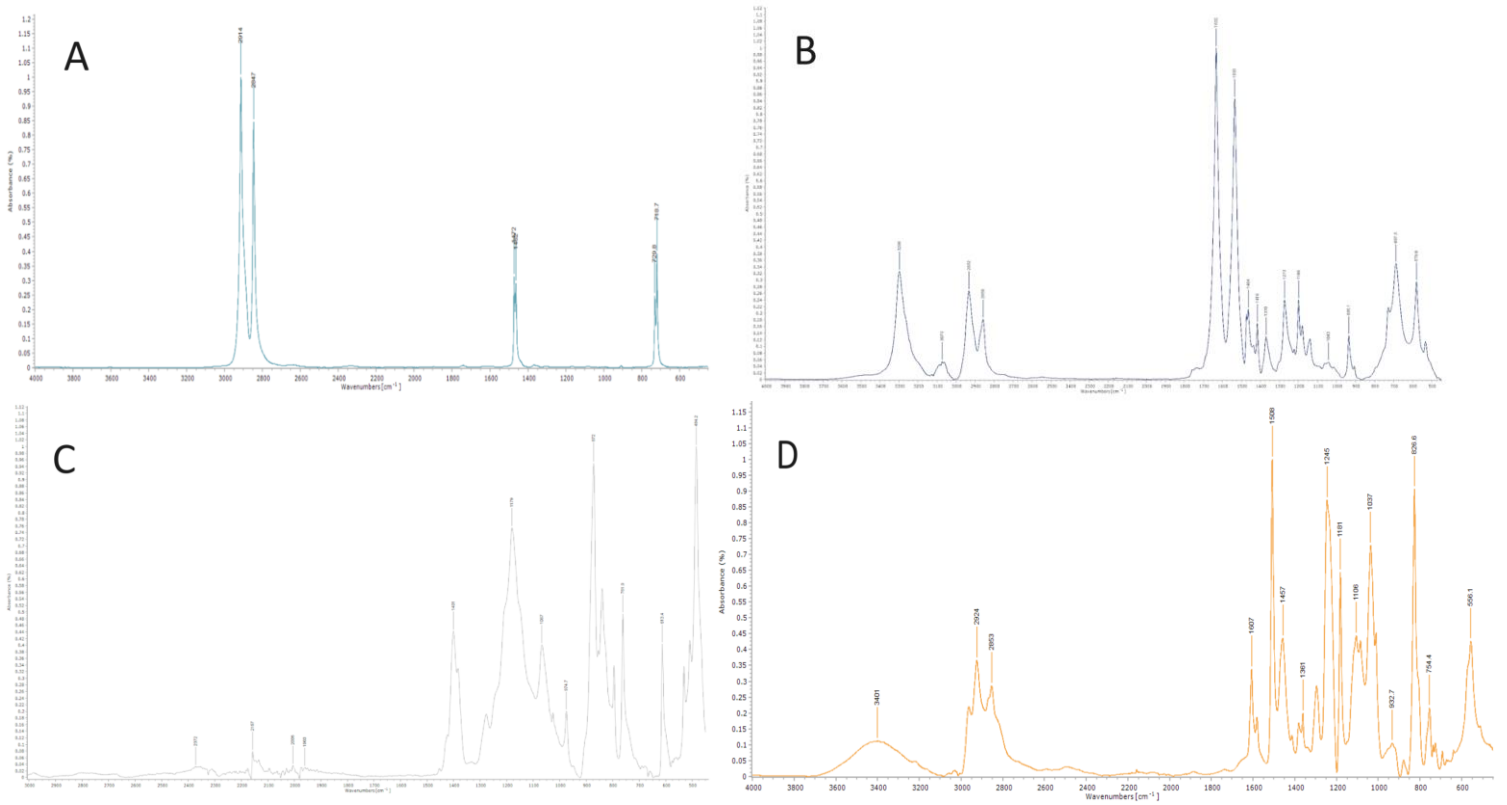


Figure 8: FTIR Spectr for HDPE(A), PA(B), PVDF(C), and epoxy(D).

Processed sheet samples were subject to cumulative scans from 4000-400 cm^{-1} and prominent peaks were highlighted. These peaks were compared to the literature for signature fingerprint regions that are unique to certain compounds and can give insights into the types of interactions in the polymer.

Several fingerprint regions were identified for the polymers such as the two smaller peaks in HDPE at 1475cm^{-1} and 725cm^{-1} . These two smaller peaks exhibit a phenomenon known as crystalline splitting which results from higher crystallinity and lack of side chains. The simple structure of polyethylene means it's FTIR spectrum will have simple but still characterizable interactions that may distinguish different similar materials.

In PVDF, the 840 cm^{-1} peak indicates the presence of a beta phase, often the result of annealing and other processing conditions. Multiple peaks also correspond to the alpha phase, a common structure found when samples have been melted and extruded.

Epoxy is the polymer that has the most sample-to-sample variation, often significantly. Our epoxy sample has generally similar FTIR spectra to other samples with a high number of peaks in the $1600\text{-}600\text{cm}^{-1}$. There is a characteristic sharp peak at around 2900cm^{-1} that corresponds to the -CH and -CH_3 bands that are prevalent in an epoxy.

3.5 2D X-Ray Diffraction

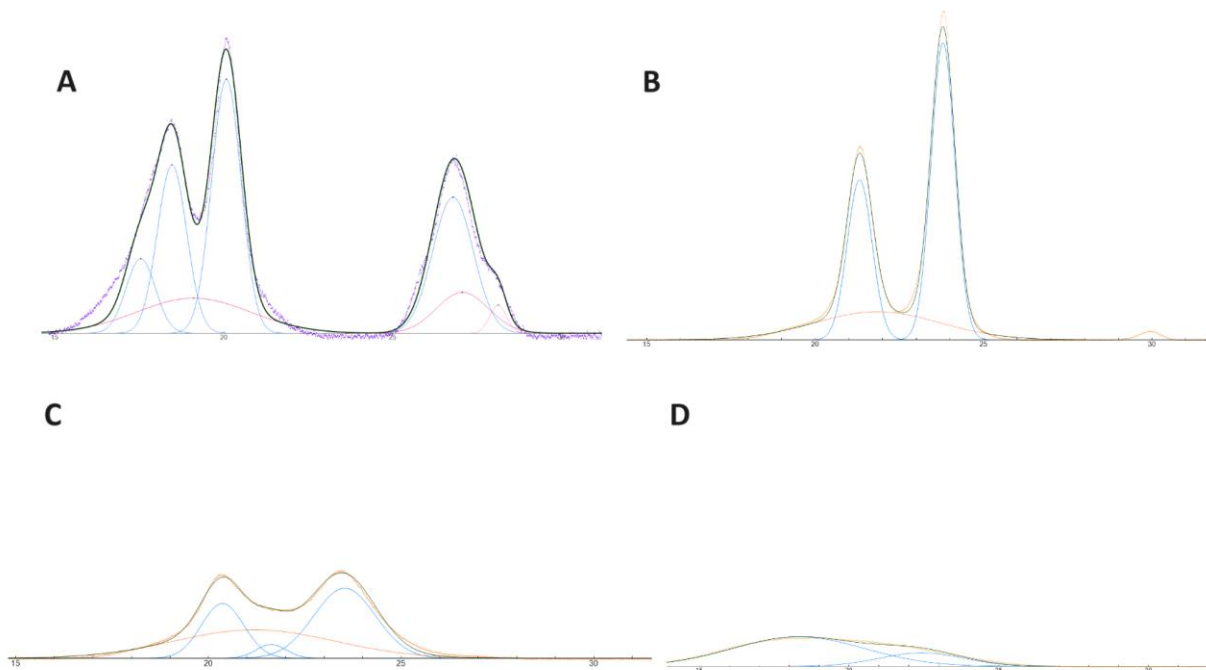


Figure 9: X-ray diffraction scan and deconvolution of (A) PVDF, (B) HDPE, (C) polyamide, and (D) epoxy.

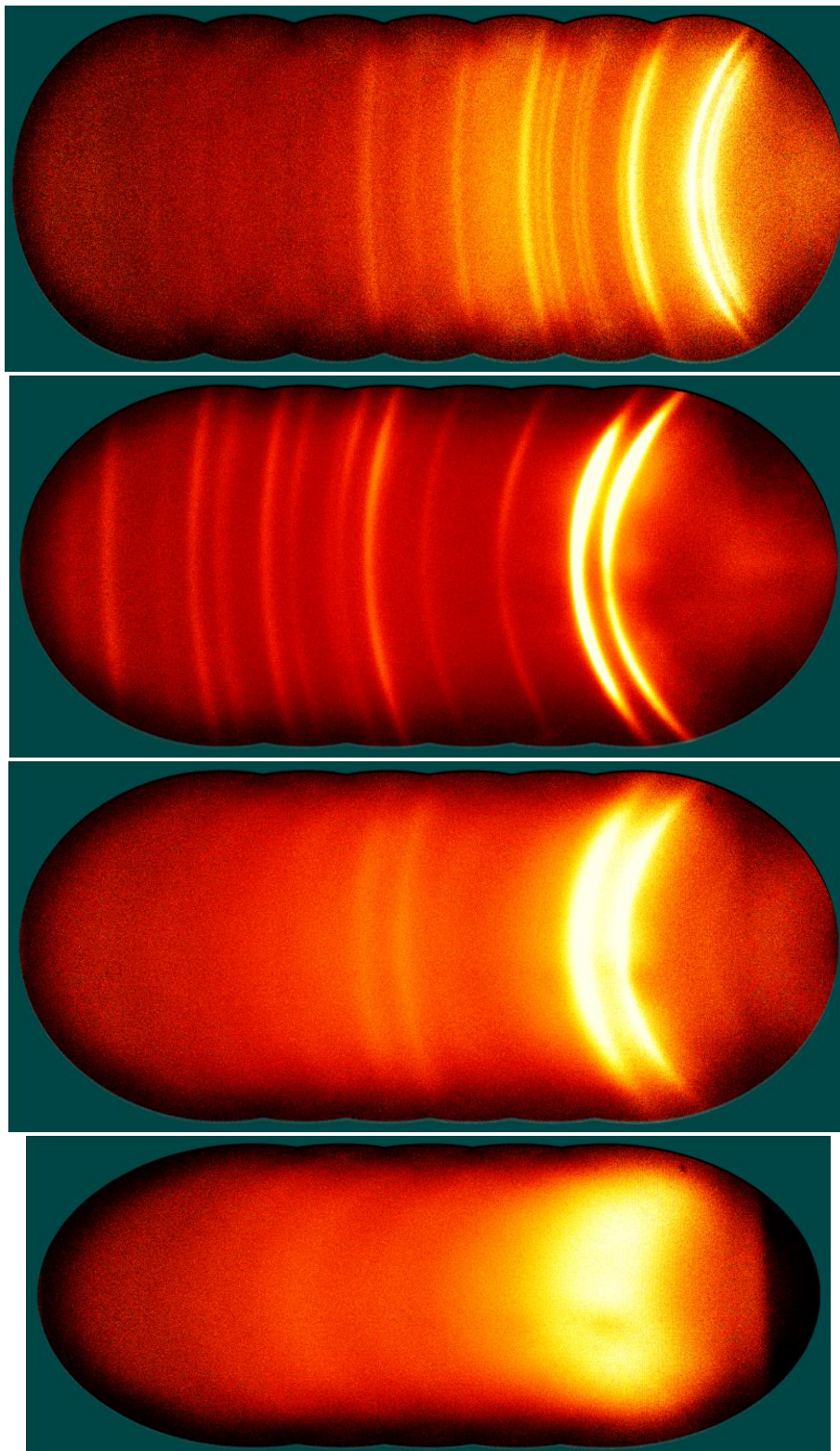


Figure 10: 2D diffraction pattern for PVDF, HDPE, polyamide, and epoxy (from top to bottom).

2D X-ray diffraction was completed on preprocessed sheets of each of the three thermoplastics and the epoxy resin. All four polymers displayed very different crystalline profiles and phase contents in their raw, unprocessed forms, but the results were consistent with those from the literature.

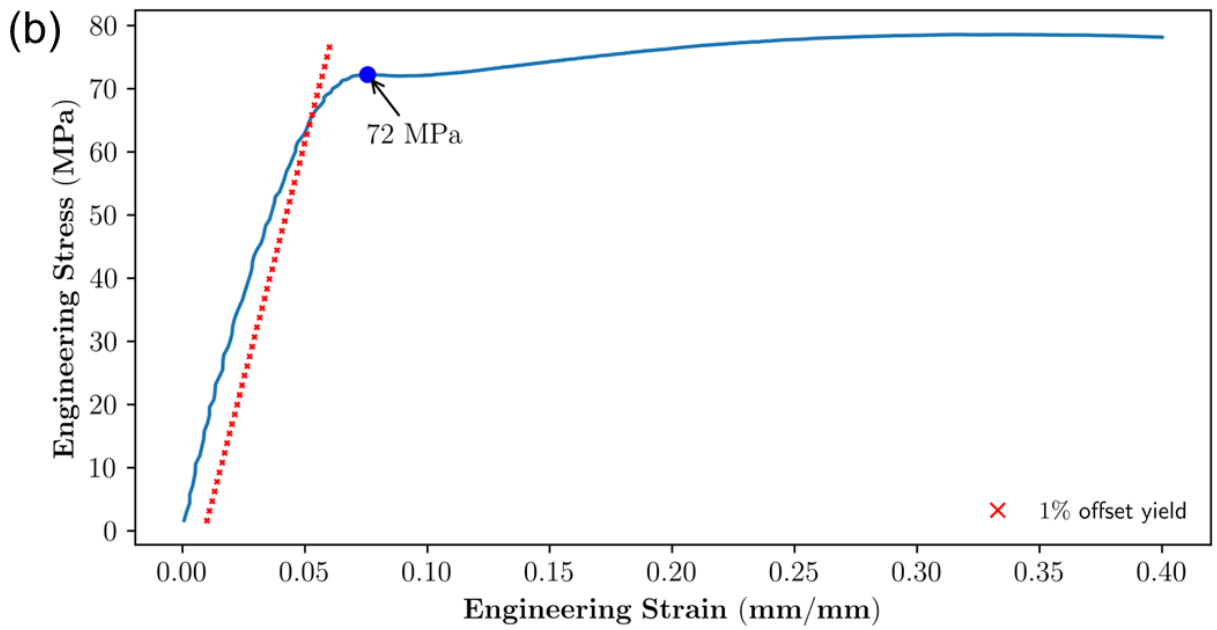
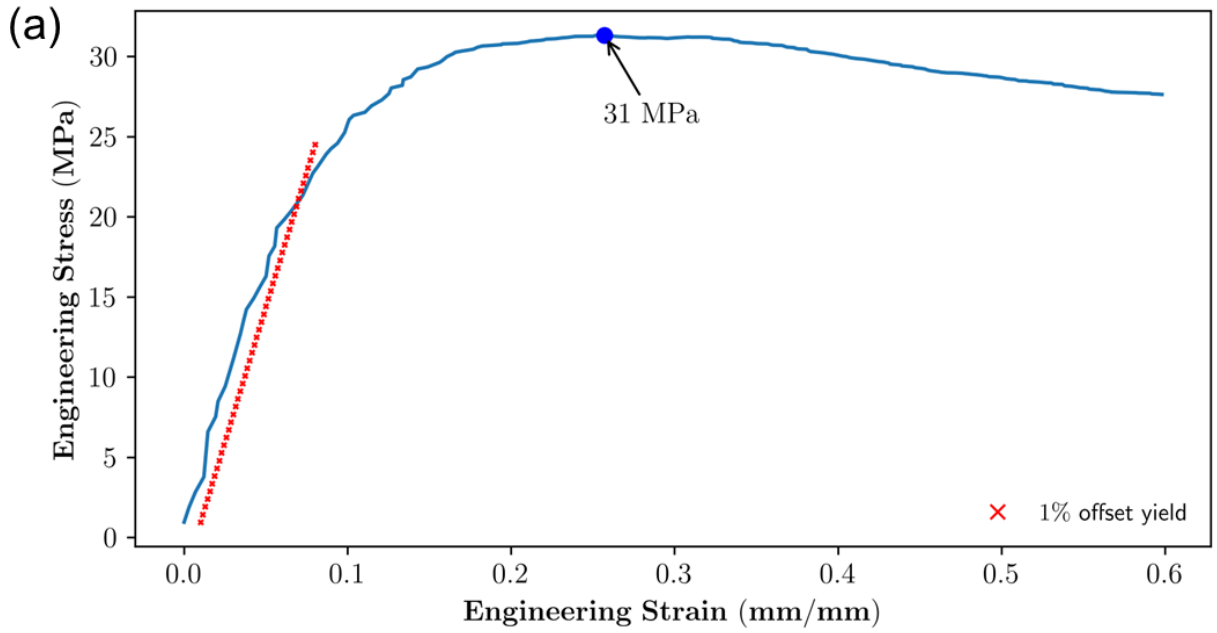
The PVDF sample has characteristic expected peaks at 20.9, 18.5, 26.8, 28.2, and 17.5 as well as 2 broader amorphous regions. These are indicative of alpha phase crystal formation, which is commonly seen in meltcast and cooled samples. Calculations of crystallinity using these regions along with the amorphous yield 76.8%. Other samples of PVDF were subject to high temperatures, pressure, and solvents to induce changes in the crystal structure. Through mechanical stretching and chemical solutions, the alpha phase was able to be transformed nearly completely into beta phase PVDF which is known to have different properties.

HDPE showed expected highly crystalline peaks at 21.3 and 23.8, along with a moderate central amorphous region. Crystallinity measures using these regions yield 75.8% crystallinity. The small peak seen at 30 degrees would normally correspond to a more oriented sample of HDPE, but due to the low intensity compared to the other peaks, there is likely minimal directional orientation in these processed samples. The flaring seen in the diffraction rings of the 2D pattern could potentially be an intermediate mesophase form, creating increased broadening in the 2 crystalline peaks.

Polyamide showed two large broader crystalline peaks at 20.4 and 23.5 and a smaller peak at 21.7. The two peaks correspond to alpha-phase crystal phases, while the single smaller peak is indicative of at least a small portion of the gamma phase. Collectively between the two different phases the crystallinity of the polyamide is 48.6%. These phases can transform into one another based on conditions like high stress or temperatures and have been shown to have effects on the mechanical properties of other materials.

The epoxy can be seen to have no crystalline peaks and can be characterized by 2 very broad amorphous regions. This can be reflected in the 2D scan, which shows no clear bands and a broad intensity region corresponding to the locations of the amorphous peaks.

3.6 Tensile Testing



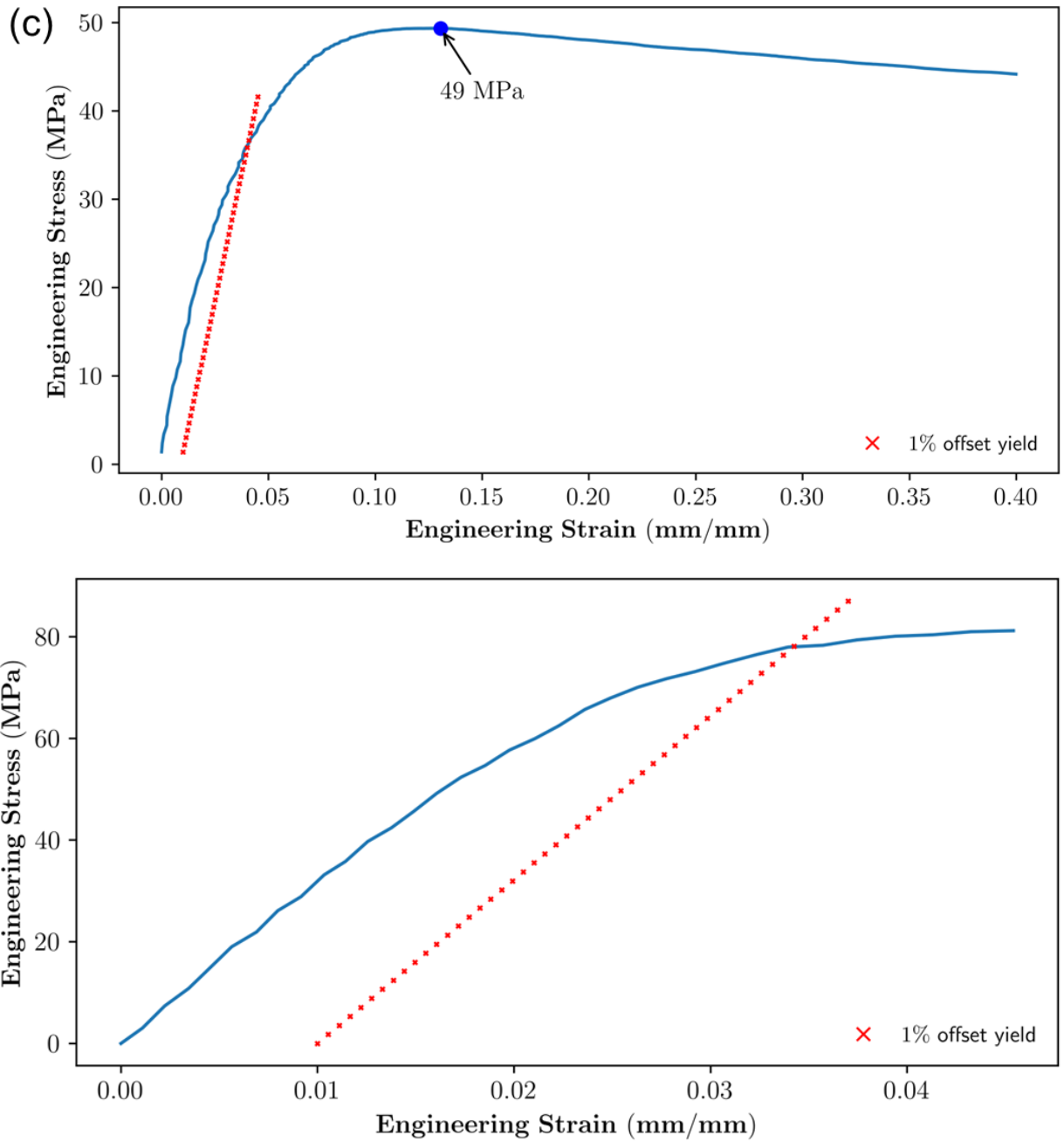


Figure 11: Engineering Stress vs Engineering Strain plots of (a) HDPE, (b) PA, (c) PVDF conducted at a strain rate of $0.0005s^{-1}$ and (d) an epoxy conducted at a strain rate of $0.0007s^{-1}$

Table 9. Mechanical properties of samples obtained from tension tests

Strain Rate = 0.0005 s ⁻¹			
	Elastic Modulus (E) (MPa)	1% offset yield strength (MPa)	σ_{max} (MPa)
HDPE	336	21	31
PA	1485	65	72
PVDF	1148	35	49
Strain Rate = 0.0007 s ⁻¹			
	Elastic Modulus (E) (MPa)	1% offset yield strength (MPa)	
Epoxy	3224	78	

We have used the 1% offset yield strength method (defined as an approximate method to estimate polymer material yield) as opposed to the 0.2% yield strength used mostly in metals. The elastic modulus is evaluated by calculating the slope of a straight line fitted to the initial elastic range.

The yield stress estimates will be instrumental in setting up the creep test load parameters. Long-term failure in HDPE is characterized by a slow crack growth mechanism. Brittle-type failure due to this mechanism occurs at stress levels of less than about half of the yield stress of the material [22]. The study of this type of failure is of importance as brittle fracture due to slow crack growth under creep is difficult to detect until the crack starts growing rapidly [29].

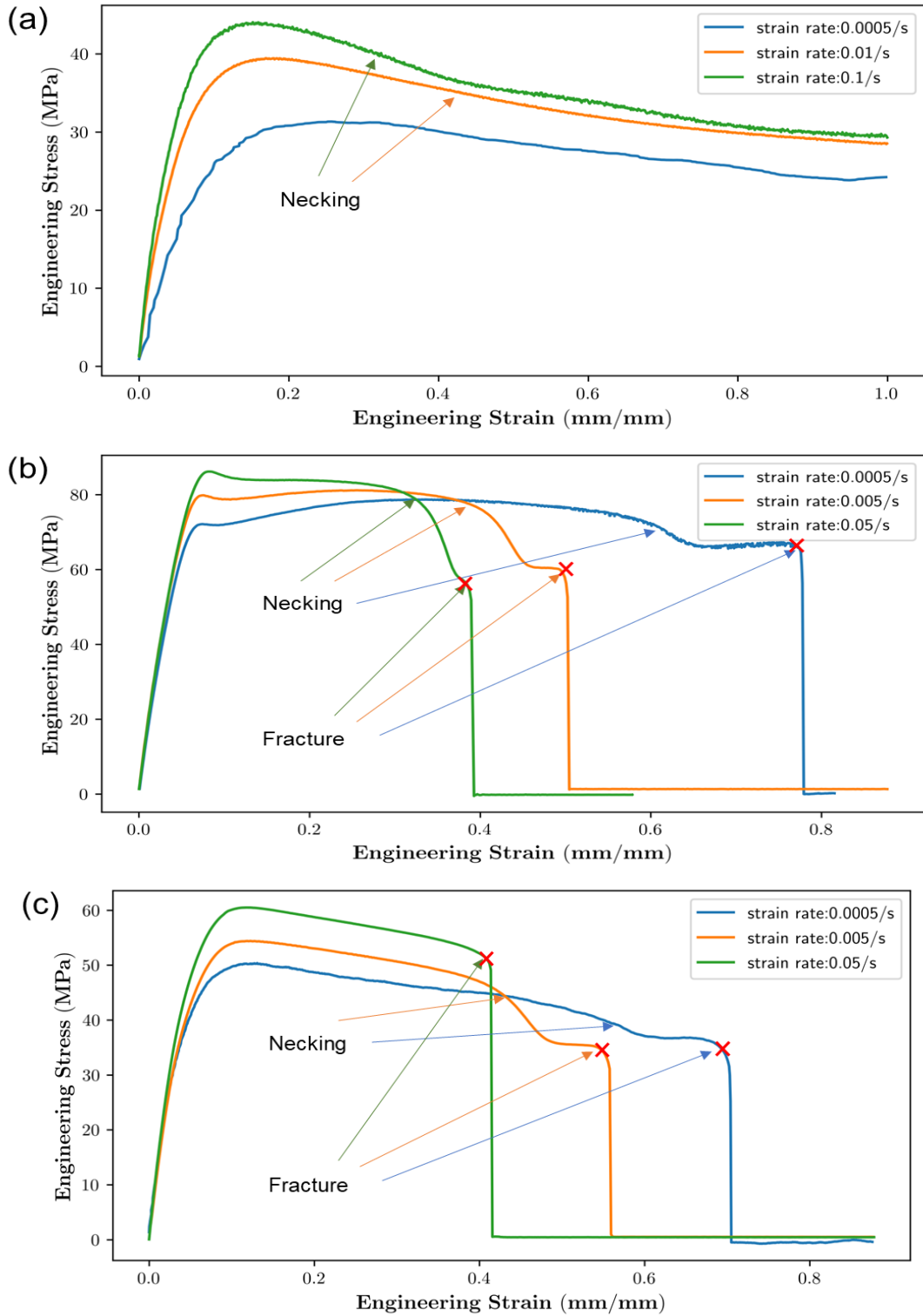


Figure 12: Rate dependence of Engineering Stress vs Engineering Strain response of (a) HDPE, (b) PA and (c) PVDF.

Tension tests were also conducted on HDPE, PA and PVDF samples at different strain rates to study their rate (inverse of time) dependent response. All 3 polymers show an increase in yield strength as the strain rate increases. HDPE samples don't fracture even till an engineering strain of 500%. At the slow strain rate of 0.0005 s^{-1} there is no visible formation of a neck for HDPE. In the PA and PVDF samples, necking followed by fracture is observed for all three strain rates. Both initiation of necking and fracture are delayed as we decrease the strain rate. The rate-dependent experimental data is useful in the calibration of a viscoelastic-viscoplastic material model.

4. Future work

There are several aspects that require further attention. Firstly, it is necessary to conduct tests on both polyamide and epoxy using the same procedure in order to determine their respective activation energies. This entails establishing a comprehensive protocol for sample preparation and applying the time-temperature-superposition principle to these materials. Additionally, samples should be subjected to aging under various conditions, including different temperatures, pressures, and gas compositions, to assess the influence of these variables on material properties, particularly their activation energies. To utilize gas compositions, it is necessary to have gas cylinders containing various gas compositions. Currently, safety protocols for handling gas cylinders are being implemented in Dr. Poling-Skutvik's laboratory, and a Standard Operating Procedure (SOP) has been developed for their use.

Additionally, like temperature, stress can accelerate the polymer dynamics and lead to rapid failure of materials. To account for this additional factor, we will use time-temperature-stress superposition, which will be an extension of standard TTS. If the complex problem of including stress in the superposition principle can be added, then in accordance with this principle, the time-dependent mechanical characteristics of viscoelastic materials under various temperatures and stress levels can be shifted along the time axis to generate a master curve at a reference temperature and stress level [24]. Polarized light microscopy is the only remaining technique that has not been tested on the polymers specified. Student training has been completed, and testing was conducted on other (trial) non-erodible polymer samples successfully. Protocols have also been established and tested successfully for hot-stage PLM testing.

We expect to begin comparing different conditioned samples under 2D-XRD and DSC in the near future. Some samples have already been created and tested, demonstrating conceptually that we can induce and detect changes in morphology.

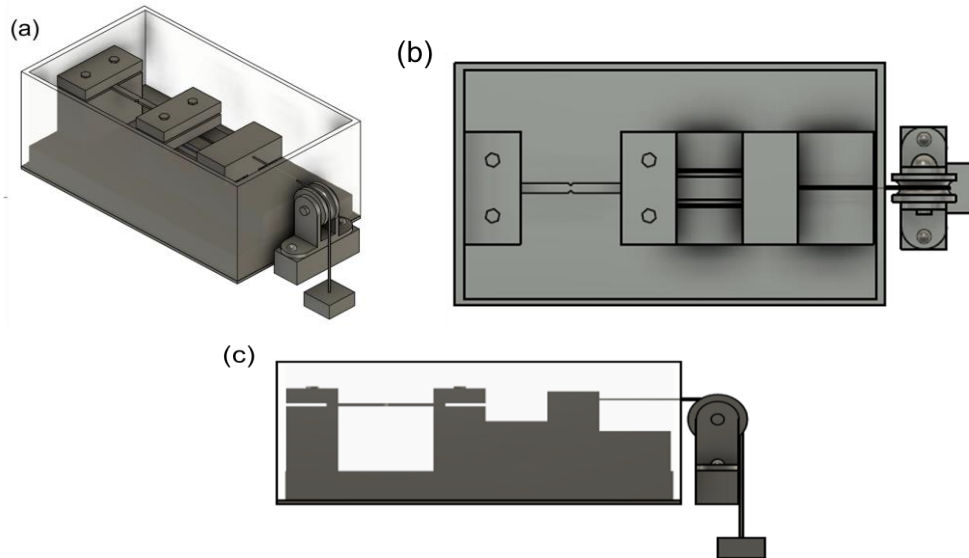


Figure 12: Schematic of the creep test setup, (a) Isometric view, (b) top view, and (c) front view.

A schematic for the design of the creep test setup has been presented in Figure 12. The tank-like structure can be used as a water bath to perform accelerated creep tests at elevated temperatures. The initial experiments will be performed on unaged samples, which will serve as a baseline for comparison with exposed liner specimens. Further, scanning electron microscopy (SEM) will be used to analyze the crack surface of the specimen's post-creep failure to better understand the effect of temperature on the morphological changes of the polymeric material.

References

- [1]. Selvakumar A, Sterling RL. State of Technology for Rehabilitation of Wastewater Collection Systems Design of Underground Facilities, View project Review of R&D in excavation technology in Japan and Europe View project [Internet]. 2010.
- [2]. Yeun J., Jung, Sunil K. Sinha. Evaluation of Trenchless Technology Methods for Municipal Infrastructure System. Journal of Infrastructure Systems [Internet]. 2007 Jun 1;13(2):144–56. Available from: [https://doi.org/10.1061/\(ASCE\)1076-0342\(2007\)13:2\(144\)](https://doi.org/10.1061/(ASCE)1076-0342(2007)13:2(144))
- [3]. Yazdekhashti S, Piratla K, Khan AA, Atamturktur S. Analysis of Factors Influencing the Selection of Water Main Rehabilitation Methods [Internet]. 2014.
- [4]. Ji HW, Yoo SS, Kim J, Koo DD. The mechanical properties of high strength reinforced Cured-in-Place Pipe (CIPP) liner composites for urbanwater infrastructure rehabilitation. Water (Switzerland). 2018 Jul 26;10(8).

- [5]. Shamsuddoha M, Djukic LP, Islam MM, Aravinthan T, Manalo A. Mechanical and thermal properties of glass fiber–vinyl ester resin composite for pipeline repair exposed to hot-wet conditioning. *Journal of Composite Materials*. 2017 May 1;51(11):1605–17.
- [6]. Orlov M v., Badeghaish WO. *Advanced Non-Metallic Coatings and Composite Materials for O & G Industry*. In: *Journal of Physics: Conference Series*. IOP Publishing Ltd; 2021.
- [7]. Li, D., Zhou, L., Wang, X., He, L., & Yang, X. (2019). Effect of crystallinity of polyethylene with different densities on breakdown strength and conductance property. *Materials*, 12(11), 1746.
- [8]. Edward, G. H. (1986). Crystallinity of linear low density polyethylene and of blends with high density polyethylene. *British polymer journal*, 18(2), 88-93.
- [9]. Androsch, R., Di Lorenzo, M. L., Schick, C., & Wunderlich, B. (2010). Mesophases in polyethylene, polypropylene, and poly (1-butene). *Polymer*, 51(21), 4639-4662.
- [10]. Bahrami, M., Abenojar, J., & Martínez, M. A. (2021). Comparative characterization of hot-pressed polyamide 11 and 12: Mechanical, thermal and durability properties. *Polymers*, 13(20), 3553.
- [11]. Dai, R., Huang, M., Ma, L., Liu, W., He, S., Liu, H., ... & Sun, A. (2020). Study on crystal structure and phase transitions of polyamide 12 via wide-angle X-ray diffraction with variable temperature. *Advanced Composites and Hybrid Materials*, 3, 522-529.
- [12]. Parodi, E., Govaert, L. E., & Peters, G. W. M. (2017). Glass transition temperature versus structure of polyamide 6: A flash-DSC study. *Thermochimica Acta*, 657, 110-122.
- [13]. Scherzer, T. (1995). Rheo-optical FTIR spectroscopy of epoxy resins. *Journal of applied polymer science*, 58(3), 501-514.
- [14]. Aboubakr, S. H., Kandil, U. F., & Taha, M. R. (2014). Creep of epoxy–clay nanocomposite adhesive at the FRP interface: A multi-scale investigation. *International journal of adhesion and adhesives*, 54, 1-12.
- [15]. Horibe, H., Hosokawa, Y., Oshiro, H., Sasaki, Y., Takahashi, S., Kono, A., ... & Danno, T. (2013). Effect of heat-treatment temperature after polymer melt and blending ratio on the crystalline structure of PVDF in a PVDF/PMMA blend. *Polymer journal*, 45(12), 1195-1201.
- [16]. Ayoub, G., Makki, M., Kadri, R., Dargazany, R., & Abdelaziz, M. N. (2024). Micromechanical modeling of the effects of crystal content on the visco-hyperelastic-viscoplastic behavior and fracture of semi-crystalline polymers. *Mechanics of Materials*, 189, 104897.
- [17]. Ayoub, G., Zaïri, F., Naït-Abdelaziz, M., & Gloaguen, J. M. (2010). Modelling large deformation behaviour under loading–unloading of semicrystalline polymers: application to a high density polyethylene. *International Journal of Plasticity*, 26(3), 329-347.

- [18]. Tripathi, A., Mantell, S., & Le, J. L. (2019). A morphology based constitutive model for high density polyethylene. *Mechanics of Materials*, 137, 103091.
- [19]. Shen, F., Kang, G., Lam, Y. C., Liu, Y., & Zhou, K. (2019). Thermo-elastic-viscoplastic-damage model for self-heating and mechanical behavior of thermoplastic polymers. *International Journal of Plasticity*, 121, 227-243.
- [20]. Challier, M., Besson, J., Laiarinandrasana, L., & Piques, R. (2006). Damage and fracture of polyvinylidene fluoride (PVDF) at 20 C: Experiments and modelling. *Engineering Fracture Mechanics*, 73(1), 79-90.
- [21]. Wiersma, J., & Sain, T. (2023). A coupled viscoplastic-damage constitutive model for semicrystalline polymers. *Mechanics of Materials*, 176, 104527.
- [22]. Hasheminejad, N.; Vuye, C.; Margaritis, A.; Van Den Bergh, W.; Direkx, J.; Vanlanduit, S. Characterizing the Complex Modulus of Asphalt Concrete Using a Scanning Laser Doppler Vibrometer. *Materials* 2019, 12 (21), 3542. <https://doi.org/10.3390/ma12213542>.
- [23]. Mohammadi, M.; Yousefi, A. A.; Ehsani, M. Thermorheological Analysis of Blend of High- and Low-Density Polyethylenes. *J. Polym. Res.* 2012, 19 (2), 9798. <https://doi.org/10.1007/s10965-011-9798-9>.
- [24]. Luo, W.; Wang, C.; Vu-Khanh, T.; Jazouli, S. Time-Stress Equivalence: Application to Nonlinear Creep of Polypropylene. *J. Cent. South Univ. Technol.* 2007, 14 (S1), 310–313. <https://doi.org/10.1007/s11771-007-0271-1>.
- [25]. Splitstone, P. L., & Johnson, W. H. (1974). The enthalpies of combustion and formation of linear polyethylene. *Journal of Research of the National Bureau of Standards. Section A, Physics and Chemistry*, 78(5), 611.
- [26]. McCollum, J., Morey, A. M., & Iacono, S. T. (2017). Morphological and combustion study of interface effects in aluminum-poly (vinylidene fluoride) composites. *Materials & Design*, 134, 64-70.
- [27]. <https://www.tainstruments.com/pdf/literature/TN048.pdf>
- [28]. N. Brown and X. Lu, A fundamental theory for slow crack growth in polyethylene, *Polymer*, 36 (3) (1995) 543–548.
- [29]. Chudnovsky, A. "Slow crack growth, its modeling and crack-layer approach: A review." *International Journal of Engineering Science* 83 (2014): 6-41.